2D Large Eddy Simulation of Turbulent Boundary Flow around a Controlled-Diffusion Wing Section Using a Locally Refined Unstructured Grid

Omar A. Qazi*, R. Prosser, S. R. Sheikh*, J. Masud*****
*College of Aeronautical Engineering
National University of Sciences and Technology, Islamabad
omar-cae@nust.edu.pk
**School of MACE, The University of Manchester, UK
***Air University, Islamabad, Pakistan.

Abstract

In this study, a 2D large eddy simulation of the flow around a thin, cambered, controlled-diffusion airfoil was carried out. An embedded local mesh refinement technique was used to achieve very fine near-wall resolution while maintaining a coarse mesh away from the airfoil. The flow was simulated at a geometric angle of attack of 8° and a Reynolds number of 1.2×10^{5}. Experimental observations show that at this angle of attack, the flow exhibits laminar leading edge separation, transition to turbulence after reattachment and vortex shedding at the trailing edge [1-3].
The embedded local mesh refinement technique was found to be very effective for selective grid refinement. A near wall resolution of $y^{+}\leq1$ and $x^{+}\leq20$ was achieved. However, the solution developed numerical oscillations with a central-difference spatial discretisation. Discontinuities existed in the velocity field at the refinement interfaces which pointed to a possible error in interpolation of velocity gradients. A stable solution was achieved with a second-order monotone scheme (MARS) available in Star-CD software. The solution reproduced all qualitative features of the flow and was found to be in good agreement with the experimental results. However, the use of the monotone scheme suppressed the small-scale turbulent structures near the trailing edge.

Keywords: Large Eddy Simulation, Turbulence, Transition

Introduction

This project was initially undertaken to investigate the feasibility of the application of LES to a particular aeroacoustic problem, i.e. the generation of broadband noise radiated from the trailing edge of a particular airfoil section. This class of airfoils were initially developed for supercritical applications in compressors, etc. In such applications, the flow can become locally supersonic [4] on the suction side of the airfoil. This leads to the generation of shock waves and subsequent separation of the boundary layer which results in lower efficiency. The controlled-diffusion airfoils induce a gradual expansion in the flow to avoid development of shock waves. In subsonic applications, the CD airfoil can avoid flow separation at the trailing edge by maintaining a favourable pressure gradient and a constant velocity over the suction side. This work is linked to the previous studies [1-3, 5-8] that include a series of wind tunnel tests and numerical simulations.

Literature review

LES is a compromise between the detailed analysis provided by DNS and the simplified approximation of the RANS approach. In LES, a filtering function is used to eliminate the small scale fluctuations, referred to as the *filtered scales*, and resolve only the larger scale motions, referred to as the *resolved scales*. The effect of the filtered scales of motion is modelled through a *subgrid scale model*. The level of detail resolved by the simulation is controlled by the filter width which is generally related to the grid resolution. The anisotropic behaviour of turbulent fluctuations in the fluid flow, e.g. in the near-wall region [9], can be resolved in LES simulations with a suitably refined computational grid.

In LES, the N-S equations are rewritten through a decomposition that is quite similar to the Reynolds decomposition in its appearance. We decompose the primary variables as, for example, $u=\overline{u}+u'$. We shall refer to this decomposition as the *filtered decomposition.* $\overline{u}$ represents the modes resolved by the simulation, referred to as the *resolved modes, and* u' represents the modes that are filtered out, referred to as the *filtered modes*. We apply the filter to the N-S equations and obtain

$$\frac{\partial\overline{u}_i}{\partial x_i}=0$$

$$\frac{\partial\overline{u}_i}{\partial t}+\frac{\partial\left(\overline{u}_i\overline{u}_j\right)}{\partial x_j}=-\frac{1}{\rho}\frac{\partial p}{\partial x_j}+2\nu\frac{\partial S_{ij}}{\partial x_j}-\frac{\partial\tau_{ij}}{\partial x_j}$$

Corresponding Author: Omar A. Qazi

The last term on the RHS of the momentum equation represents the effect of the filtered modes, and the term τ_{ij} is referred to as the *subgrid scale stress.* The higher modes in a turbulent flow drain the kinetic energy of the lower modes in the energy cascade but the filters in LES eliminate these higher modes from the simulation. A *subgrid scale model* is then used to reconstruct the subgrid scale stresses to maintain the proper momentum balance. This reconstruction of subgrid stresses is based on the properties of the resolved flow field and correct modelling of the subgrid scale stresses is important for accurate LES.

The sub-grid scale stress τ_{ij} is defined [10-12] as

$$\tau_{ij} = \overline{u_i u_j} - \overline{u}_i \overline{u}_j$$

By using the decomposition relation for resolved and filtered modes, the RHS can be expanded as

$$\begin{aligned}\overline{u_i u_j} &= \overline{(\overline{u}_i + u_i')(\overline{u}_j + u_j')} \\ &= \overline{\overline{u}_i \overline{u}_j} + \overline{\overline{u}_i u_j'} + \overline{u_i' \overline{u}_j} + \overline{u_i' u_j'}\end{aligned}$$

Which leads to

$$\begin{aligned}\overline{u_i u_j} - \overline{u}_i \overline{u}_j = {} & \overline{\overline{u}_i \overline{u}_j} - \overline{u}_i \overline{u}_j && \textit{(Leonard Stress)} \\ & + \overline{\overline{u}_i u_j'} + \overline{u_i' \overline{u}_j} && \textit{(Cross Stress)} \\ & + \overline{u_i' u_j'} && \textit{(Reynold's Stress)}\end{aligned}$$

In the Reynolds decomposition used in RANS simulations, Leonard stress and cross stress terms reduce to zero due to the statistical properties of the decomposition.

$$\overline{\overline{u}_i \overline{u}_j} - \overline{u}_i \overline{u}_j = 0$$
$$\overline{\overline{u}_i u_j'} + \overline{u_i' \overline{u}_j} = 0$$

This is not the case in filtered decomposition. In most subgrid scale models, the effect of the three stresses is modelled as a whole through an eddy-viscosity hypothesis, as used in the RANS modelling. However, it is important that the subgrid scale model should be Galilean invariant, which is also a property of the N-S equations. Speziale showed that even though cross and Leonard stresses do not have Galilean invariance, their sum is Galilean invariant. Therefore, a subgrid scale model which models their sum as a whole, must also exhibit this property.

LES filters

In LES, the flow variables are filtered by using a convolution integral [11, 12] such that

$$\overline{u}(\mathbf{x},t) = \int G(\mathbf{r},\mathbf{x})\, u(\mathbf{x}-\mathbf{r},t)\, d\mathbf{r}$$
$$where \int G(\mathbf{x},\mathbf{r})\, d\mathbf{r} = 1$$

The convolution integral in fact acts as a low-pass filter, that allows the lower modes to pass through and eliminates the high modes. Typical filters defined in the literature for use in LES are as following [11]:

Fourier cut off filter $$G(\kappa) = \begin{cases} 1 \; if \; \kappa \le \pi/\Delta \\ 0 \; otherwise \end{cases}$$

Gaussian filter $$G(x) = \left(\sqrt{\frac{6}{\pi\Delta^2}}\right) exp\left(-\frac{6x^2}{\Delta^2}\right)$$

Top hat filter $$G(x) = \begin{cases} 1/\Delta \; if \; |x| \le \Delta/2 \\ 0 \; otherwise \end{cases}$$

The Fourier cut-off filter is defined in wave number space and is the only one of the above filters that affects the small scales only, i.e. it eliminates all modes higher than the cut-off wave number, and leaves the lower modes unchanged. The other filters are defined in physical space and affect a range of length scales around the filter width to varying degrees. However, McMillan & Ferzieger [13] observed that the choice of filter has only a minor effect on results.

An important requirement for LES filters is that they should be commutative and mean-preserving in the computational domain. In the case of non-uniform spatial discretisation, the filter width varies in the domain. Ghosal & Moin [14] highlighted that the LES filters are mean-preserving and commutative only for uniform grids. Ghosal [15] showed that in case of non-uniform grids, the choice of filter may introduce errors of the order of $\mathbf{\Delta^2}$. In the finite volume formulation of LES, the filter is implicit in the spatial discretisation; most subgrid scale models use the volume of the computational cell to compute filter width. This implies that the resolved modes in a finite volume based LES may be contaminated, especially with non-uniform grids.

Smagorinsky subgrid model

Our simulation was based on the Smagorinsky model which uses the Prandtl mixing length hypothesis [16] to estimate the value of turbulent viscosity. Smagorinsky related the mixing length to the grid filter width [12] by the relation

$$l_m = C_s \Delta$$

In the above expression $\mathbf{\Delta}$ is the filter width and is related to the grid size. C_s is the *Smagorinsky constant*. Its value is adaptable for various flows and is generally in the

range of C_s =*0.1 – 0.2* [11]. The eddy viscosity can be computed from the rate of strain at the resolved scale by the relation

$$\nu_T = (C_s\Delta)^2\left|\bar{S}\right|$$

$\left|\bar{S}\right|$ is the magnitude of the strain rate of the resolved eddies so that

$$\left|\bar{S}\right| = \sqrt{2\bar{S}_{ij}\bar{S}_{ij}}$$

The eddy viscosity predicted by the model is directly proportional to the resolved strain rate. However, the model cannot distinguish between laminar and turbulent flows. Its prediction of the eddy viscosity depends only on the value of strain rate computed from the resolved modes. In laminar flow regions with high velocity gradients, the model may predict subgrid scale stresses and can corrupt the resolved mean flow in the laminar region. Dahlstrom [17] conducted LES for the transitional[1] flow over a high lift airfoil. He noted that the prediction of subgrid scale stresses results in reduced mean flow values in the laminar region. This can affect the transition phenomenon as well as the characteristics of the turbulent boundary layer that forms after the transition. Huai et al [18] noted that the additional dissipation introduced by the subgrid scale model can delay, or even inhibit the transition to turbulence. This observation is of importance to our study since accurate prediction of transition has a direct affect on reattachment of flow at the leading edge.

Van-Driest damping

The Smagorinsky model predicts high values of subgrid stresses in the near-wall region. Van Driest [19] proposed a logarithmic damping of the Smagorinsky constant in the near-wall region based on viscous wall units. This damping function also forces the sub-grid scale stresses to vanish at a solid boundary. The damping function is as following

$$C_{S_m} = C_s\left[1 - e^{y^+/A^+}\right]^2$$

y^+ is the wall-normal distance measured in the viscous wall units and A^+ is a constant with a default value equal to 26. The viscous wall unit is defined as

$$y^+ = \frac{u_\tau y}{\rho}$$

where

$$u_\tau = \sqrt{\frac{\tau_w}{\rho}}$$

[1] Transition from laminar boundary layer to turbulent boundary layer

Laminar-turbulent transition

The prediction of laminar turbulent transition is a considerable challenge for LES. Huai et al [20] state that the transition to turbulence in a spatially developing boundary layer initiates as two dimensional, laminar disturbances. These perturbations lead to the development of 3D disturbances which transform into small scale motions in the final stage of transition. In numerical simulations, there is no excitation mechanism to emulate the natural transitional behaviour of the fluid. This makes it difficult to duplicate the transition process accurately in a numerical simulation.

Dahlstrom [21] observed that in numerical simulations of transitional flow over an airfoil, the numerical oscillations in the solution tend to introduce transition to turbulence. There is no physical correlation to the manner in which transition is initiated in the numerical solutions. However, the results appear to relate favourably to the physics of the flow. The challenge is to control the non-physical, oscillatory behaviour in the numerical simulation in a manner that allows the correct prediction of the transition phenomena. These can be controlled by the initial / boundary conditions, the choice of numerical scheme and selection of the computational domain.

Grid generation

The governing principles of LES and subgrid scale modelling highlight the importance of suitable grid resolution in these simulations. The filter width is computed directly from the cell volume, which is then used to compute the local eddy viscosity and the local subgrid stresses. Coarse grids can result in over-prediction of the subgrid stresses. The choice of the grid resolution is, therefore, vital in the application of LES. Baggett et al [9] quantified the near-wall resolution required for LES, and stated that the anisotropic stresses are important in the near-wall and in free-shear dominated regions. They directly affect the mean shear stresses and the mean velocity profiles. These stresses are not represented in eddy-dissipation models even though they are very important in the near-wall region. Baggett et al state that the integral length scales of turbulence must dictate the grid spacing near the wall, to resolve properly all the length scales associated with anisotropic eddies. The integral dissipation length is given as

$$L_\varepsilon \approx \frac{k^{1.5}}{\varepsilon}$$

Baggett et al [9] show that the number of grid cells in a fluid volume required to resolve all anisotropic modes, can be approximated by

$$N_T \approx \int_{y_o}^{\infty}\frac{(\Delta L)^3}{y^3}dy \approx \frac{(\Delta L)^2}{y_o^2}$$

ΔL is a characteristic length of the fluid volume and is a dimension that represents the length scale of the largest isotropic eddies. By representing the length y_o in terms of viscous wall units $y_o = \frac{\nu}{u_T} y^+$, it can be shown that the number of anisotropic modes scale with the square of Reynolds number.

Previous research

Roger & Moreau [1, 2, 7] conducted experiments on the Valeo-CD airfoil in an open-jet wind-tunnel experiment. The velocity, pressure and sound pressure levels for various flow conditions were collected. An important observation in these experiments was that the flow characteristics for the airfoil in an open-jet wind tunnel were quite different from the free stream conditions [1]. The installation effects in the experiment modified the flow in a manner that could not be correlated to free stream flow behaviour by an angle of attack correction or any other method. This necessitated that the simulation should incorporate the installation geometry to resolve the features resulting from installation effects.

Moreau et al [2] conducted a 2D RANS simulation of the full experimental domain as shown in Fig. 1 (from Moreau et al [2]). They concluded that the mean flow showed good agreement with the experimental results. Fig. 1 shows that there is a large deflection of the jet core as the flow passes over the airfoil. The airfoil is located in the unexpanded core of the jet which imposes a different pressure loading than the free steam conditions. This effect has been discussed in Moreau et al [1].

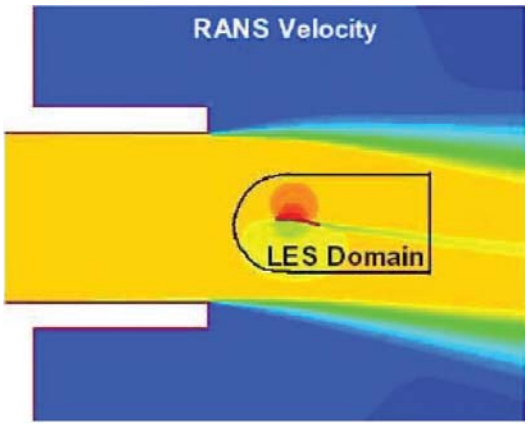

Fig. 1. 2D RANS Simulation Domain of Experimental Setup (Moreau et al [2])

Methodology

Domain selection

LES requires much finer computational grids than RANS, especially in the near-wall region. Therefore, an LES analysis of the full experimental geometry would be computationally expensive. An alternate approach would be to cut out a sub-domain from the RANS domain of Fig. 1. Moreau et al [2] extracted a smaller sub-domain, as shown in Fig. 1, for LES. The boundary conditions would be extracted from the mean flow obtained from the RANS results. The same approach is being used in this study. The domain used for the LES simulation is the same as that used by Moreau et al [2] for ease of comparison. The domain geometry and boundary conditions used in this study are also the same and have been provided by Moreau. The flow is simulated for a 13.5 cm chord length and at 8° geometric angle of attack. The flow velocity is 16 m/s which corresponds to a Reynolds number of 1.2×10^5 based on the airfoil chord length.

In the actual simulation, the inlet velocity was normalised to achieve a free stream velocity of 1 m/s. The airfoil chord length was scaled to 10 cm. The dynamic similarity of the numerical simulation with the experimental setup was achieved by scaling the viscosity to maintain the actual flow Reynolds number. This rescaling allowed the specification of a larger time-step in the transient simulation while maintaining a suitable Courant number. We may highlight that this rescaling also affects the pressure term in the incompressible momentum equations. The absolute value of pressure is rescaled by factor of $(U_n/U)^2$. U is the actual free stream velocity while U_n is the rescaled free stream velocity.

Grid generation

The two important aspects of grid generation in our case were the near-wall resolution, and the refinement from the domain boundaries towards the airfoil. The airfoil geometry is shown in Fig. *2*.

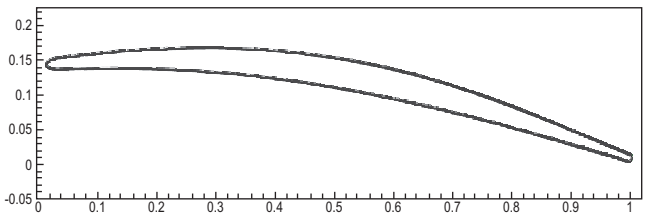

Fig. 2. Airfoil Geometry

Experimental results [1-3, 5, 7, 17] show that the flow remains laminar all over the airfoil surface, except in a part of the boundary layer on the suction side, and in the airfoil wake. On the airfoil suction side, a small laminar separation bubble is formed at the leading edge followed by laminar reattachment [1]. The laminar boundary layer transitions into turbulence in the later half of the airfoil suction side. We expect to see very little separation of the mean boundary layer at the trailing edge. The instantaneous flow field may exhibit a transient, and possibly periodic, separation phenomenon under the combined effect of turbulence and vortex shedding at the trailing edge.

Cell aspect ratios

The references [9, 11, 21, 22] approach the determination of minimum grid resolution for turbulent boundary layers with different perspectives. In most cases, they concentrate on resolving a particular type of flow. Dahlstrom [21] reports satisfactory results for transitional flows over a high-lift airfoil with $y^+ = 0.8$ and $x^+ = 220$. Piomelli [11] suggests $y^+ < 1$ and $x^+ \approx 50-150$ to represent accurately the turbulent structures. We concluded that the maximum cell dimensions must be maintained at $y^+ < 1$ and $x^+ \leq 20$ in viscous wall units. The wall-normal dimension was adjusted by specifying the grid expansion factor and the total number of wall-normal cells in the domain.

Grid generation method

Star-CD software presents a number of options for generating computational grids [23, 24]. We did not use the automatic mesh generation methods available, so that the grid generation and refinement process could be manually fine-tuned to the prescribed resolution requirements.2D LES is carried out by generating a one-cell wide computational grid with symmetric boundaries in the spanwise direction. The domain was divided into five zones as shown in Fig. 3. For each zone, or *patch*, the number of cells in the streamwise and normal direction was specified. The number of cells in the streamwise direction was kept to a minimum in each patch at this time. The only consideration was to reproduce correctly the airfoil geometry. In the wall-normal direction, an algebraic expansion was incorporated to affect gradual coarsening of the mesh away from the airfoil. The *expansion factor*[2] was important in this step. If the grid was expanded too quickly, there was a chance of producing numerical oscillations or wiggles in the solution with central differencing scheme. On the other hand, slower expansion would make it difficult to maintain the desired aspect ratios for grid cells. This will be explained further with the introduction to *embedded local mesh refinement*. There was no guideline available on determination of an appropriate expansion factor. After trial and error, we concluded that the most appropriate value was 1.075, i.e. 7.5% cell height increase in successive layers. Our final grid uses this expansion factor. The same expansion factor was used in all four *patches* (1-4) around the airfoil (in Fig. 3) to ensure proper coupling at the interfaces.

Grid refinement

Locally refined meshes are generated when one cell face overlaps whole or part of the faces of more than one neighbouring cells. This group of computational cells is known as a couple. The cell whose single face interacts with the faces of more than one cells, is known as the master cell, while the other cells in the couple are called the slave cells. However, the interpolation of properties at the coupled faces is no longer a simple process, especially in regions where steep gradients exist in fluid properties. The coupling of one master cell with more than two slave cells is not preferred due to this reason. The major advantage of using embedded local refinement is that the grid can be selectively refined in the required regions while maintaining a coarse mesh in other parts of the domain. However, it introduces a large, sudden jump in grid resolution which may have an adverse effect on the solution. Further investigation is required into the effects of such a refinement on LES solutions.

The final grid included six levels of refinement from the domain boundary towards the airfoil surface. Each level of refinement represents a two-fold increase in the number of cells per layer[3], moving from the domain boundary towards the airfoil. The reason is that by using integral coupling in the stream wise direction, one *master* cell couples with two slave cells in the adjacent layer. (Fig. 4) shows a closer view of the refinements near the airfoil. It can be seen that the refinement is localised to a very small region around the airfoil and the major part of the domain has a coarse mesh.

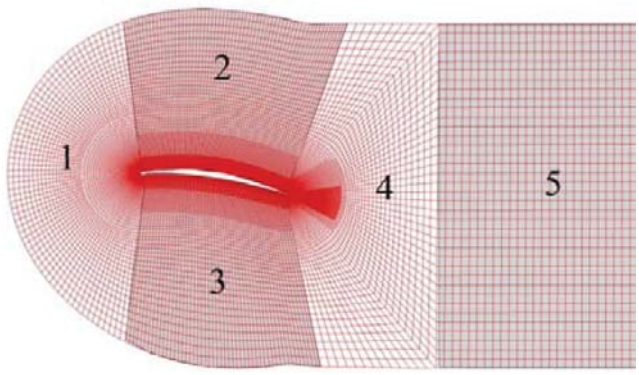

Fig. 3. Grid zones

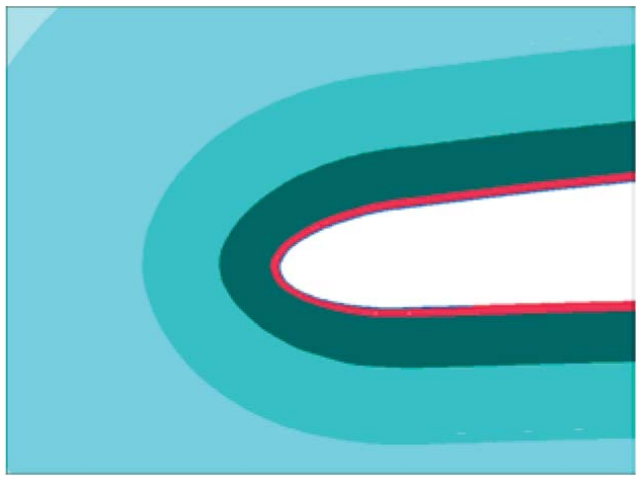

Fig. 4. Grid refinement close to airfoil surface

[2] Ratio of wall-normal dimension of cells in adjacent layers $\Delta y_{k+1}/\Delta y_k$.

[3] The layer of cells equidistant from airfoil surface in the normal direction to the airfoil surface.

Fig. 5 shows the cell geometry and the cell refinement around the airfoil leading edge. It can be seen that the grid around the leading edge becomes coarser very quickly as we move away from the airfoil. The main considerations were to reproduce properly the leading edge geometry and to have adequate resolution in the wall-normal direction, to resolve the laminar boundary layer.

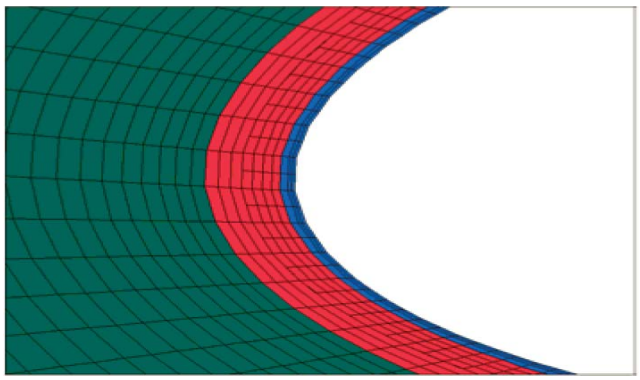

Fig. 5. Grid refinement around the airfoil leading edge

Results and discussion

Our approach in the use of embedded local meshes was to achieve computational economy by tailoring the grid to the characteristics of the flow. In our final grid, 80-85% of the cells are located within the boundary layer and the turbulent wake. Throughout this region, the grid has been refined to the levels at which we expect to resolve all the flow characteristics with reasonable accuracy. A large part of the flow in our computational domain is laminar and has been allocated only about 15% of the total grid cells. We used a body-fitted refinement around the airfoil that would allow regular cell geometry all around the airfoil in the boundary layer region. The matching with domain boundaries was done outside this region. Fig. 6 shows instantaneous pressure contours from LES which are in qualitative agreement with the reference simulations by Moreau et al.

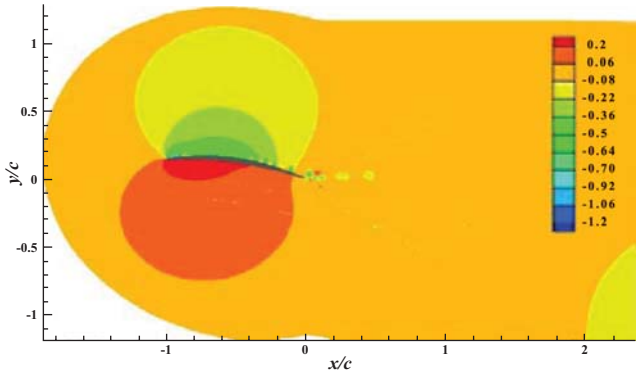

Fig. 6. Pressure contours

Fig. 7 shows a closer view of the grid around the trailing edge. The difference in refinement criteria on the airfoil pressure and suction sides is visible

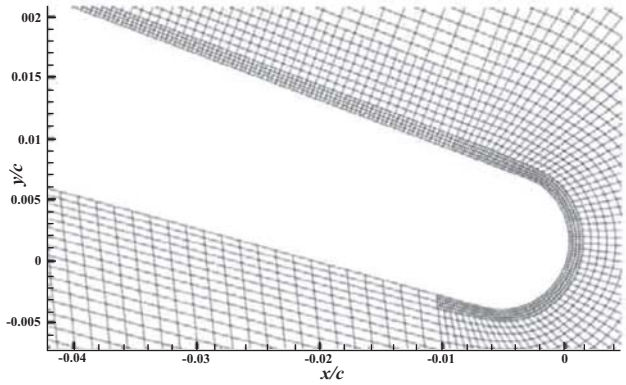

Fig. 7. Close-up view of trailing edge

Fig. 8 and Fig. 9 show the velocity magnitude and pressure contours respectively. The flow shows good agreement with the experimental and RANS results of Moreau et al [1-3]. The velocity contours show a well-defined leading edge separation bubble. Regular vortex shedding is observed from the separation bubble. The vortices convect downstream along the suction side surface. The vortices in this case do not lose their strength since there is no vortex stretching phenomenon. This phenomenon also results in higher velocities in the vortex cores than in the physical or 3D case. A flattening of the vortices is observed around the airfoil mid-chord. The 2D vortices again start to gain strength as the flow encounters the convex curvature leading to the trailing edge. The pressure contours also highlight these aspects. The flow remains attached throughout the airfoil length.

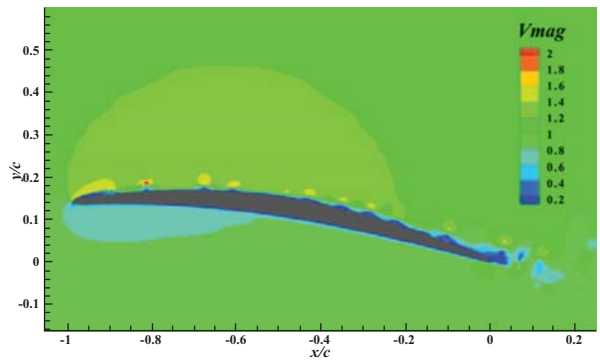

Fig. 8. Instantaneous velocity plot

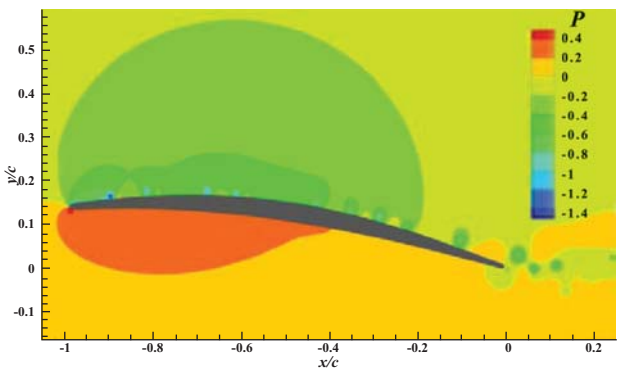

Fig. 9. Instantaneous pressure plot

Fig. 10 shows the eddy viscosity computed by the subgrid scale model in the domain. The highest level of the eddy viscosity predicted near the airfoil is almost an order of magnitude lower than the molecular viscosity of the fluid. This showed that the near-wall grid could adequately resolve the near-wall turbulent structures.

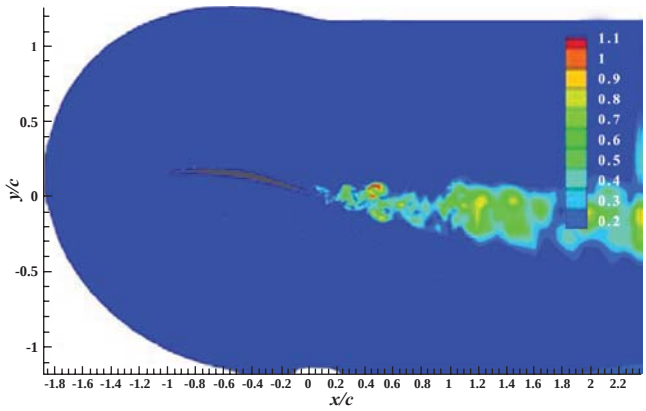

Fig. 10. Contour plot of normalised instantaneous eddy viscosity

A close-up view of the velocity vectors in the leading edge separation bubble is shown in Fig. 11. We see that the vortices grow within the separation bubble until they gain sufficient strength to break off from the rear end of the separation bubble. A detached vortex can also be seen in this figure as it travels on the airfoil suction side. We observed that these vortices seemed to detach from the separation bubble at a regular frequency. Fig. 12 shows a sequence of vortices on the airfoil surface near the trailing edge that has travelled from the leading edge. The vortices display some restructuring near the trailing edge under the influence of the slight adverse pressure gradient seen in Fig. 9. In the airfoil wake, we can see the interaction of these vortices with the vortex shedding from the trailing edge. The upper vortex generated at the trailing edge blends with the vortices travelling from the leading edge separation bubble.

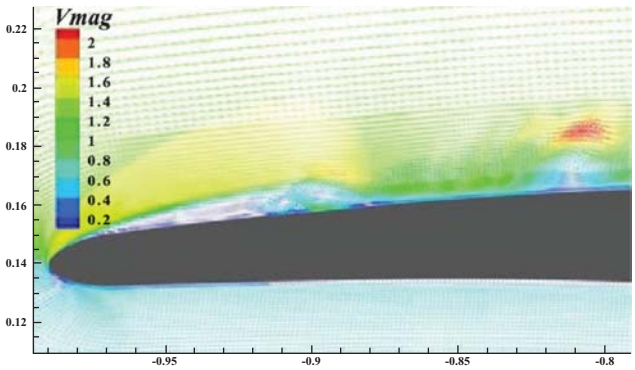

Fig. 11. Velocity vectors at the airfoil leading edge

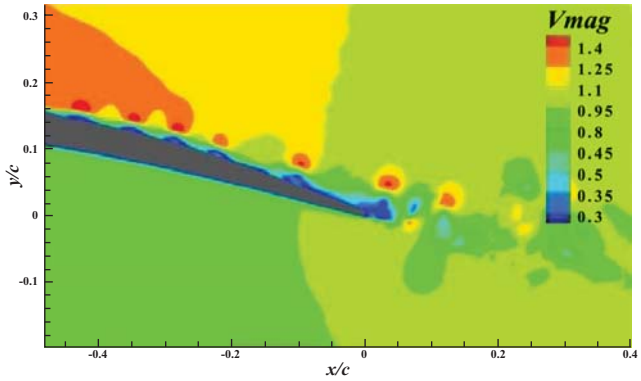

Fig. 12. Vortex shedding at the trailing edge

The periodicity of this phenomenon is exhibited by the monitored values of the primary variables just upstream of the trailing edge as shown in Fig. 13. The dominant signals in this figure have a frequency of around 250 Hz. This observation is supported by the experimental results of Roger and Moreau et al [1-3, 5, 7] where broadband noise ranging from 400 Hz to 1 KHz were recorded. Experimental evidence of vortex shedding from the leading edge separation bubble has also been recorded.

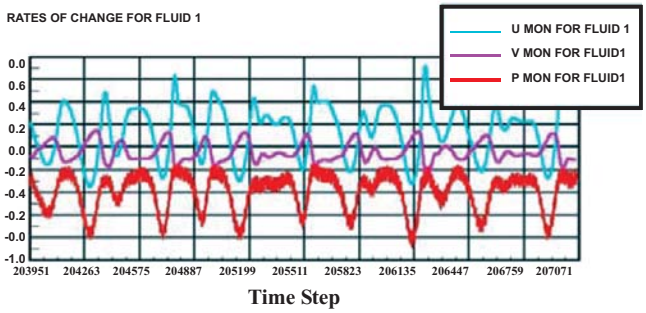

Fig. 13. History of monitored flow variables near the trailing edge

Findings

In this study, we attempted to identify the limits within which an LES of highly turbulent boundary layer flow could be carried out with sufficient accuracy for industrial applications. We used a systematic method to identify the important factors in the grid generation process with embedded local meshes. The instability of the solution was one of the major concerns in our study. Our results indicate that a stable solution cannot be achieved with embedded refinement technique while using the central-difference scheme. We found evidence to show that the flow field and its first gradients are discontinuous across the interfaces of the embedded refinement. This discontinuity leads to the development of numerical oscillations that destabilise the flow.

The only mode for suppression of the numerical oscillations tested in our study has been the use of the MARS scheme. This scheme uses a TVD method to control the appearance of new extremes in the solution. The scheme proved to be more effective in cases when the oscillations seemed to be more pronounced in the coarser cells. The use of this scheme in this case led to solution stability. Our study has highlighted that in the near-wall region, there are many governing factors for the development of numerical oscillations. These include the effects of grid expansion factor, embedded local refinement and the grid resolution. The effect of each of these factors has to be investigated more thoroughly to understand the performance of the MARS scheme. It would also be interesting to study the effectiveness of explicit flux limiting in providing a stable solution to such problems.

Fig. 14 shows the C_p values plotted against the normalised chord length. The result obtained from our simulation are compared with the experimental results and the LES results of Moreau et al [2]. The obvious difference is the prediction of a larger separation bubble at the leading edge in our study. The pressure recovery after the separation bubble is at the correct level. The prediction for the rest of the airfoil is also in good agreement with the experimental results.

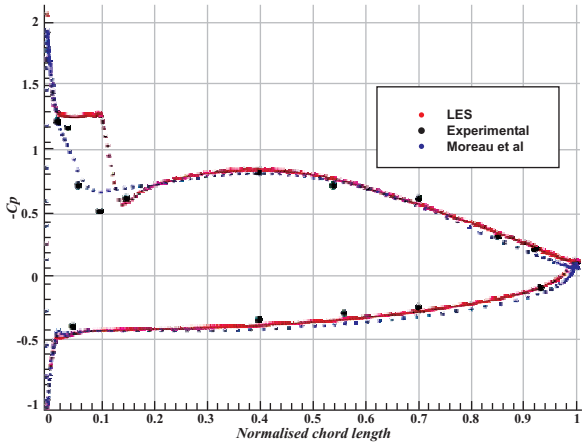

Fig. 14. Comparison of C_p with experimental data

We noted that the higher values and peaks of C_p are indicative of the stronger strength of the travelling vortices. The separation also seems to be over-predicted. The Smagorinsky model is known to be too dissipative. In the detached shear layer, it adds significant amount of artificial viscosity that can delay the onset of turbulence. Van Driest damping is also known to be relatively ineffective in separated flows. These factors combined with improper near-wall resolution can lead to over-prediction of separation.

Conclusion

Our study has highlighted that a combination of embedded local mesh refinement technique and LES offers a promising approach for turbulent boundary layer simulation of external aerodynamic flows at moderate to high Reynolds numbers. We have shown that sufficient near-wall resolution can be obtained for industrial applications at low computational cost. This was not the first application of embedded local refinement with LES. Similar work has previously been carried for fully turbulent internal flows [25]. Our application of this technique to external aerodynamic flows has highlighted that mesh discontinuities raise new issues in the presence of transition and a uniform / potential flow. At the same time, future directions have been identified to resolve these problems. Successful resolution of these issues will open a whole new field of aerodynamic applications for LES.

REFERENCES

1. S. Moreau, M. Henner and M. Roger, "Analysis of flow conditions in freejet experiments for studying airfoil self-noise", *AIAA*, Vol. 41, No. 10 2003, pp. 1895-1905.
2. S. Moreau, D. Neal and J. Foss, "Hot wire measurements around a CD airfoil in an open-jet anechoic wind tunnel", *ASME Heat Transfer/Fluid Engineering Summer Conference,* 2004, Charlotte, North Carolina, USA.
3. S. Moreau and M. Roger, "Effect of airfoil aerodynamic loading on trailing edge noise", *AIAA*, 2003. pp. 3225.
4. B. Song, *Experimental and numerical investigations of optimized high-turning supercritical compressor blades*, Virginia Polytechnic Institute and State University, 2003, pp. 155.
5. M. Roger and S. Moreau, "Trailing edge noise measurement and prediction for subsonic loaded fan blades", *AIAA*. 2002.
6. M. Roger and S. Moreau, "Broadband fan noise prediction using single-airfoil theory-Part 1: Theoretical background", *Fan Noise*, 2003.
7. M. Roger and S. Moreau, "Broadband self-noise from loaded fan blades", AIAA, Vol. 42, No.3, 2004, pp. 536-544.
8. M. Roger, S. Moreau and A. Guedel. "Broadband fan noise prediction using single-airfoil theory-Part 2:Experimantal validation", *Fan Noise*, 2003.
9. J. S. Baggett, J. Jimenez, and A. G. Kravchenko, "Resolution requirements in large-eddy simulations of shear flows", *Centre for Turbulence Research: Annual Research Brief*, 1997, pp. 51-66.
10. J. H. Ferziger and M. Peric, *Computational Methods for Fluid Dynamics*. 3rd, rev. ed. New York: Springer, 2002, pp. 423.
11. U. Piomelli, "Large-eddy and direct simulation of turbulent flows", *CFD2001 - 9 e conférence annuelle de la Société canadienne de CFD, 2001*, Kitchener, Ontario.
12. S. B. Pope, *Turbulent Flows*, Cambridge University Press, 2000, pp. 771.
13. O. J. McMillan and J. H. Ferziger, "Direct testing of subgrid scale models", *AIAA*, Vol. 17 No. 12, 1979, pp.1340-1346.
14. S. Ghosal and P. Moin, "The basic equations for the large-eddy simulation of turbulent flows in complex-geometry", *Journal of Computational Physics*, Vol. 118, 1995. pp. 24-37.

15. S. Ghosal, "An analysis of numerical errors in large-eddy simulations of turbulence", *Journal of Computational Physics,* Vol. 125, 1996, pp. 187-206.
16. J. A. Ligget, *Fluid Mechanics*, International ed. Mc-Graw Hill, 1994, pp. 532.
17. S. Dahlstrom and L. Davidson, "Large-eddy simulation of the flow around an airfoil", *39th AIAA Aerospace Sciences Meeting and Exhibit*, 2001, Reno, NV, USA.
18. X. Huai, S. R. D. Joslin, and U. Piomelli, "Large-eddy simulation of boundary layer transition on swept wings", *Journal of Fluid Mechanics*, Vol. 381, 1999, pp. 357-380.
19. E. R.Van Driest, "On turbulent flow near a wall", *Journal of Aerospace Sciences*, Vol. 23, 1953.
20. X. Huai, R. D. Joslin, and U. Piomelli, "Large-eddy simulation of transition to turbulence in boundary layers", *Theoretical and Computational Fluid Dynamics*, Vol. 9 1997, pp. 149-163.
21. S. Dahlstrom, *Large-Eddy Simulation of Flow Around a High-lift Airfoil*. Goteborg, Sweden, Chalmers Reproservice, 2003,
22. J. S. Baggett, "On the feasibility of merging LES with RANS for the near-wall region of attached turbulent flows", *Centre for Turbulence Research: Annual Research Briefs*, 1998, pp. 267-277.
23. CD-adapco, Star CD v 3.20 User Guide. 2004.
24. CD-adapco, Star CD v 3.20 methodology manual. 2004.
25. Y. Addad, "Large-Eddy Simulations of Bluff Body, Mixed and Natural Convection Turbulent Flows with Unstructured FV Codes", *Mechanical, Aerospace and Manufacturing Engineering*, UMIST: Manchester, 2005.